PROCEEDINGS, Twenty-Ninth Workshop on Geothermal Reservoir Engineering
Stanford University, Stanford, California, January 26-28, 2004
SGP-TR-175

EXPERIMENTAL STUDY OF TWO-PHASE FLOW STRUCTURE EFFECTS ON RELATIVE PERMEABILITIES IN A FRACTURE

Chih-Ying Chen[1], Roland N. Horne[1] and Mostafa Fourar[2]

1. Department of Petroleum Engineering, Stanford University, Stanford, California 94305, USA
e-mail: alnchen@stanford.edu, horne@stanford.edu
2. Ecole Nationale Supérieure des Mines de Nancy – LEMTA, Parc de Saurupt, 54042 Nancy Cedex France
e-mail: fourar@mines.inpl-nancy.fr

ABSTRACT

Two-phase flow through fractured media is important in geothermal, nuclear, and petroleum applications. However, the knowledge of the relationship between flow behavior and relative permeabilities is limited. In this research, an experimental apparatus was built to capture the unstable nature of the two-phase flow in a smooth-walled fracture and display the flow structures under different flow configurations in real time. The air-water relative permeability was obtained from experiment and showed deviation from the X-curve behavior suggested by earlier studies. Through this work the relationship between the phase-channel morphology and relative permeability in fractures was determined. A physical tortuous-channel approach was proposed to quantify the effects of the flow structure. This approach could replicate the experimental results with a good accuracy. Other relative permeability models (viscous-coupling model, X-curve model and Corey-curve model) were also compared. Except for the viscous-coupling model, these models did not interpret the experimental relative permeabilities as well as the proposed tortuous-channel model. Hence, we concluded that the two-phase relative permeability in fractures depends not only on liquid type and fracture geometry but also on the structure of the two-phase flow.

1 INTRODUCTION

Multiphase flows through fractured porous media are of great importance in several domains such as petroleum recovery, geothermal energy and environmental engineering. In the case of two-phase flow in a single fracture, this importance extends to several industrial processes such as compact heat exchanges and nuclear engineering. Despite this importance, few theoretical and experimental studies have been devoted to establishing the laws governing these flows. Thus, the results presented in the literature seem to be in contradiction. So far, the mechanisms of two-phase flows in a fracture are not well understood and a general model for describing these flows is still not determined.

The approach used commonly to describe two-phase flow in a fracture is the relative permeability concept, which is based on a generalization of the Darcy equation. Three models for the relative permeabilities are presented in the literature: the X-model (straight lines), the Corey model, and the viscous-coupling model. The experimental results presented in the literature also show different behavior for the relative permeabilities. Some results are in accordance with the X-model whereas other results are in accordance with the Corey-model or the viscous-coupling model.

Although the flow structures are of a great importance in modeling two-phase flows, the three models do not take into account these effects. The purpose of this paper is to examine the effects of the flow structures on the relative permeabilities during two-phase flow in a single fracture. The paper is organized as follows: in Section 2, we present a review of the theoretical and experimental approaches for two-phase in a fracture. In Section 3, we describe the experimental apparatus and the measurements of pressure drops, flow rates, and saturations. In Section 4, we describe the observed flow structures and calculated relative permeabilities. In Section 5, we propose a tortuous-channel approach and discuss the flow structure effects on relative permeabilities. Finally, in Section 6, we outline the main conclusions of this study.

2 BACKGROUND

In this section, we present the main theoretical models for relative permeabilities in a single fracture. Then, we discuss some experimental results from the literature.

2.1 Theoretical Approaches

The commonly used equations to model steady-state laminar two-phase flow in a single fracture are the generalized Darcy equations:

$$u_l = \frac{k_{abs} k_{rl} (p_i - p_o)_l}{\mu_l L} \quad (1)$$

$$u_g = \frac{k_{abs} k_{rg} (p_i - p_o)_g}{\mu_g L} \quad (2)$$

where subscripts l and g stand for liquid and gas, respectively; p_i and p_o are the pressures at the inlet and the outlet of the fracture; u is the superficial velocity or the Darcy velocity (flow rate per unit of section area); μ is the dynamic viscosity; L is the fracture length; k_{abs} is the absolute permeability and k_{rl} and k_{rg} are the relative permeabilities of the liquid and the gas, respectively.

To take the compressibility effect of the gas into account, Equation (2) must be rewritten in the following form (Scheidegger, 1974):

$$u_g = \frac{k_{abs} k_{rg} (p_i^2 - p_o^2)}{2\mu_g L p_o} \quad (3)$$

The absolute permeability of a smooth-walled fracture is related to the fracture aperture, b, by (Yih, 1969: Eq. 341; Witherspoon et al., 1980):

$$k_{abs} = \frac{b^2}{12} \quad (4)$$

The concept of the relative permeability provides us a means to quantify the relative resistance or interference between phases. For liquid-gas flow, the sum of k_{rl} and k_{rg} indicates the extent of phase interference: the lower the sum of the relative permeabilities below 1, the greater the phase interference. The critical point of the generalized Darcy model is the determination of the relative permeabilities, which are usually supposed to be only functions of the saturation. When the pressure loss due to the interaction between phases is negligible against the pressure loss due to the flow of each fluid, the relative permeabilities can be modeled by the X-curves:

$$k_{rl} = S_l \quad (5)$$

$$k_{rg} = S_g \quad (6)$$

where S_l and S_g are the liquid and gas saturation respectively.

According to X-model, the sum of k_{rl} and k_{rg} equals 1, which means the absence of phase interference. Physically this implies that each phase flows in its own path without impeding the flow of the other. In fractures, if each phase flows via perfect straight channels along the flow direction with negligible capillary pressure and wetting-phase stratified flow, then X-curve behavior is possible. However, for two-phase flows through a real fracture, the surface contact between the two fluids can be important and, consequently, the interaction between the two fluids may not be negligible. As the fracture flow can be considered either as a limiting case of a flow in a porous medium (Pruess and Tsang, 1990) or as a limiting case of a pipe flow (Fourar et al., 1993), there are mainly two approaches for modeling relative permeabilities.

In the porous media approach, the fracture is treated as a connected two-dimensional porous medium where the pore space occupied by one phase is not available for the flow of the other phase. A phase can move from one position to another only upon establishing a continuous flow path for itself. The competition for pore occupancy is controlled by the capillary pressure. Based on this approach, several numerical studies were performed (Murphy and Thomson, 1990; Rossen et Kumar 1994, Mondoza et Sudick, 1991, Pyrak-Nolte et al. 1992). The main result is that the sum of k_r is less than 1 and, consequently, the X-model is not suitable to describing the numerical calculations of the relative permeabilities as functions of the saturation. However, these studies do not establish theoretical relationships for k_r. The shape of the curves obtained was more similar to the curves obtained in classical porous media, namely the Corey curves (Corey, 1954):

$$k_{rl} = S^{*4} \quad (7)$$

$$k_{rg} = (1 - S^*)^2 (1 - S^{*2}) \quad (8)$$

In these equations, S^* is the saturation defined by:

$$S^* = (S_l - S_{rl}) / (1 - S_{rl} - S_{rg}) \quad (9)$$

where subscript r refers to residual saturation. The Corey model represents strong phase-interference in comparison with the X-model.

The pipe flow approach is based on the observation that flow structures observed in a fracture show more similarity to the structures observed in a pipe than to those expected for a porous medium (Fourar and Bories, 1995). These flow structures show strong interference between the two fluids flowing simultaneously. However, the real mechanisms are very difficult to model because the geometry of the interface between the fluids is unknown and one of the phases is generally discontinuous. Fourar and Lenormand (1998) assumed that the complexity of the real flow can be modeled, in a first

approximation, by viscous coupling between the fluids. The fracture is then modeled by two parallel planes with a small aperture. The two fluids are flowing simultaneously and the interface is assumed to be planar. Fluid *l* is considered as the wetting fluid and therefore is in contact with the walls, and fluid *g* (nonwetting) flows in between. The viscous coupling between fluids is derived by integrating Stokes' equation for each stratum. Identification of the established equations and the generalized Darcy equations leads to:

$$k_{rl} = \frac{S_l^2}{2}(3 - S_l) \tag{10}$$

$$k_{rg} = (1 - S_l)^3 + \frac{3}{2}\mu_r S_l (1 - S_l)(2 - S_l) \tag{11}$$

where $\mu_r = \mu_g/\mu_l$ is the viscosity ratio.

These equations show that the relative permeability of the nonwetting fluid depends on the viscosity ratio μ_r. k_{rg} can be larger than unity when $\mu_r > 1$ (lubrication effects). However, for gas and liquid two-phase flows, $\mu_r << 1$ and, consequently, the second term in the right-hand-side of Equation (11) is negligible.

2.2 Experimental Approaches

Several studies on two-phase flows in a fracture have been performed. Romm (1966) studied kerosene and water two-phase flow through an artificial fracture by using parallel glass plates. The surface of each plate was lined with strips of polyethylene or waxed paper. The strips divided the entire fracture into 10 to 20 narrow parallel fractures (2-3 mm width) with alternate wettability.

Persoff et al. (1991) and Persoff and Pruess (1995) also performed experiments on gas and water flow through rough-walled fractures using transparent casts of natural fractured rocks. The study of Persoff et al. (1991) showed strong phase interference similar to that in porous media. In these experiments, flow of a phase was characterized by having a localized continuous flow path that undergoes blocking and unblocking by the other phase.

Diomampo (2001) performed experiments of nitrogen and water flow through smooth-walled artificial fractures. She also observed the intermittent phenomenon in her experiments. Furthermore, her results conform mostly to the Corey type of relative permeability curve. This suggests that flow through fractures can be analyzed by treating it as a limiting case of porous media flow and by using the relative permeability approach.

Fourar et al. (1993) and Fourar and Bories (1995) studied air-water two-phase flow in a fracture constituted of two parallel glass plates (1m x 0.5 m) with an opening equal to 1 mm. The injector consisted of 500 stainless steel tubes of 1 mm outside diameter and 0.66 mm inside diameter. Air and water were injected through alternating capillary tubes to achieve uniform distribution of the inlet flow. For all experiments, air was injected at a constant pressure and its volumetric flow rate was measured by a rotameter and corrected to the standard pressure. Water was injected by a calibrated pump. At the outlet of the fracture, the gas escaped to the atmosphere and the water was collected.

The fracture was initially saturated with water which was injected at a constant flow rate for each experiment. Air injection was then started and increased stepwise. When the steady state was reached for each flow rate, the pressure drop and the saturation were measured. The pressure drop was measured by a transducer and the saturation was measured by using a balance method. Then, the fracture was resaturated with water and the experiment was repeated several times at different liquid flow rates. This study has been extended to fractures constituted by bricks made of baked clay (30 cm x 14 cm) with different apertures (0.54 mm, 0.40 mm and 0.18 mm).

Results obtained in these various studies are presented in Figure 1 in terms of k_{rg} versus k_{rl}. As can be seen, experimental results obtained by Romm (1966) are well described by the X-model, that is the relative permeability of each phase equals to its saturation. On the other hand, the relative permeablities obtained by Fourar and Bories (1995) are rather in accordance with the viscous-coupling model. However, the results obtained by Diomampo (2001) are well described by the Corey model. Lastly, the results obtained by Persoff and Pruess (1995) show more interaction between phases than the other results. It is obvious that these previous studies show a diversity of behavior of relative permeabilities in fractures. Furthermore, less attention has been paid to study the relationship between flow structures and relative permeabilities. Although the flow structure from the experimental study performed by Romm (1966) is not reported, it is likely that it was a channel flow due to the fracture configuration (alternate wetting and nonwetting stripes). In this case, the interaction between phases is minimum and, consequently, the results are described by the X-model. The experiments performed by Persoff et al. (1995) showed that the flow is characterized by having a localized continuous flow path that is undergoing blocking and unblocking by the other phase. This behavior is related to capillary effects, which are dominant in classical porous media. Consequently, the flow of

one phase is strongly impeded by the flow of the other phase. In the experiments performed by Fourar and Bories (1995), several flow structures were observed: bubbles, fingering bubbles, drops and films. It seems that these flows are dominated by viscous forces.

The purpose of this study is to visualize and discuss the two-phase flow behavior in a fracture. The obtained gas-water relative permeabilities are analyzed by examining the flow structures. Finally a tortuous-channel approach is developed to reproduce experimental results and to show the effect of the flow structures on the relative permeabilities.

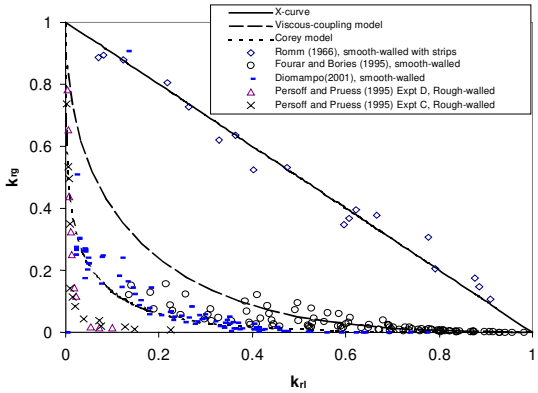

Figure 1. Compendium of previous measurements of relative permeabilities in fractures (Romm (1966) results from kerosene-water flow, the rest were air-water or nitrogen-water flow).

3 EXPERIMENTAL APPARATUS AND MEASUREMENTS

In this study, gas-water flow experiments were conducted at 24°C. The fluids consisted of pure nitrogen and deionized water. The water injection was controlled by a meter pump (Dynamax, SD-200, rate: 0.1-200 ml/min). Gas injection was controlled through a flow regulator (Brooks Instrument, Flow Controller Model 0151E), which was connected to a gas meter (Brooks Instrument, Flow Meter model 5850E, max. rate: 200 ml/min). All measurements were electronic and digitized by using high-speed data acquisition system (DAQ; National Instrument, SCSI-1000 with PCI 6023E A/D board) and digital video recording system (Sony Digital-8 560X with Pinnacle Studio DV IEEE 1394 image capture card). The whole experimental system is illustrated in Figure 2, which shows the fluid supply, the fracture apparatus, data acquisition system, and digital image recording. In this section, we first describe the fracture apparatus. Then we describe the pressure, flow rates, saturation measurements, and data processing method.

3.1 Fracture Apparatus Description

The fracture is created by a smooth glass plate on top of an aluminum plate confined by a metal frame bolted to the bottom plate. The aperture of the fracture was set to 130 μm by using stainless steel shims along the flow boundaries. The schematic view and photograph of the fracture apparatus are shown in Figure 3. An O-ring (Viton 1/8" thick #2-272) was placed in between the glass and aluminum plate as a seal. The fluids enter into the fracture through two separate canals. Each canal has several ports drilled in a way that they align on the surface (see Figure 3). The surface of the fracture apparatus was designed such that there is an available 12 inch by 4 inch space for flow. Throughout this flow area, tiny pressure ports were drilled so as to minimize surface discontinuity. Four pressure ports were drilled along the fracture as shown in Figure 3. The two-phase fluid exits through a single outlet. The apparatus was designed to be of sufficient length to minimize the capillary end effects.

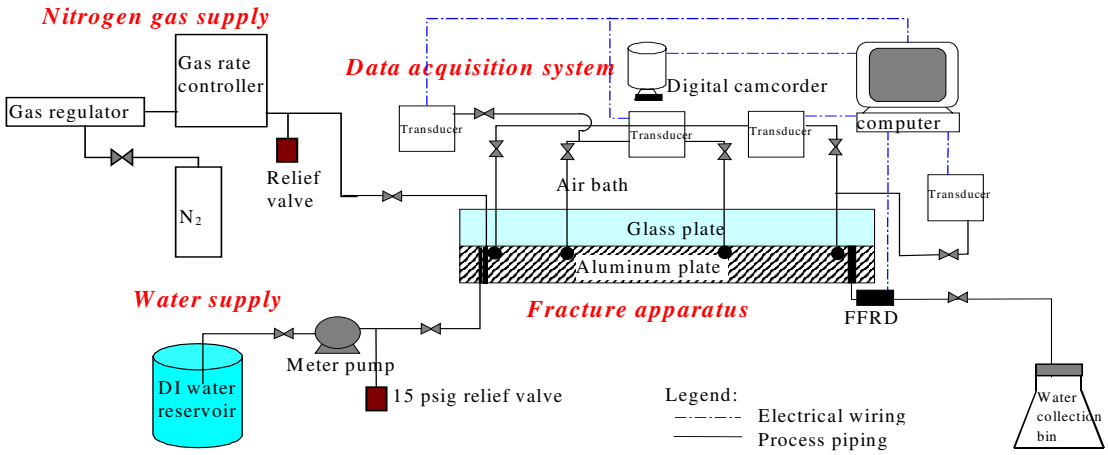

Figure 2. Process flow diagram for air-water experiment.

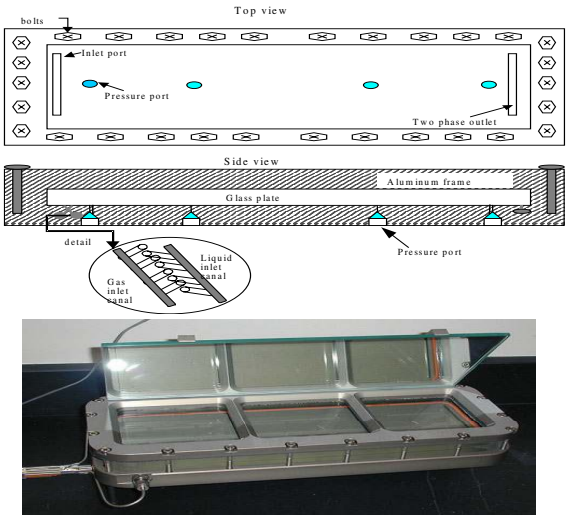

Figure 3. Schematic diagram and picture of fracture apparatus.

3.2 Pressure Measurements

Low-range differential transducers were used to measure the pressure difference through the fracture, as well as the intermediate pressure and the two-phase outlet pressure. Two liquid differential transducers (Validyne Transducer, model DP-15, range 0-2 psig) were attached to four pressure ports inside the fracture to measure the pressure difference through the fracture. Another transducer (Validyne Transducer, model DP-15, range 0-5 psig) was attached to the middle point of the fracture. The fourth transducer (Validyne Transducer, model DP-15, range 0-5 psig) was attached to the two-phase outlet of the fracture apparatus. These transducers send electrical signals to the data acquisition system, which was monitored using the LabView® programmable virtual instrument software. The complete measurement configuration in the fracture apparatus is shown in Figure 2.

3.3 Flow rates Measurements

Aside from the known input rates, to obtain the instantaneous flow rates, a fractional flow ratio detector (FFRD) was designed and constructed as shown in Figure 4a. The FFRD was used to measure the outlet gas and water fractional flows, f_g and f_w.

$$f_g = \frac{q_{out,g}}{q_{out,t}} \quad \text{and} \quad f_w = \frac{q_{out,w}}{q_{out,t}} \tag{12}$$

$$q_{out,t} = q_{out,w} + q_{out,g} \tag{13}$$

where $q_{out,g}$ is the outlet gas flow rate, $q_{out,w}$ is the outlet water flow rate, and $q_{out,t}$ is the outlet total flow rate. The principle of the FFRD is that different phases will have different refractive indices. A phototransistor (NTE 3038, NPN-Si, Visible) was installed inside the FFRD, producing different voltages when sensing different strengths of light. The water phase produces a higher voltage when flowing through the FFRD as shown in Figure 4b. The gas and water phase flow ratios are obtained by determining the ratio of the number of gas and water signals. Once f_g and f_w are obtained at steady-state condition, it is easy to calculate $q_{out,g}$ in Equation (12) by assuming that water flow rate remains constant from inlet to outlet of the fracture. This assumption can hold if the wetting phase, water, flows in a continuous channel, and the water viscosity is much larger than the nonwetting phase. The calibration of the FFRD demonstrated a good linearity between measurement and actual values (Figure 5).

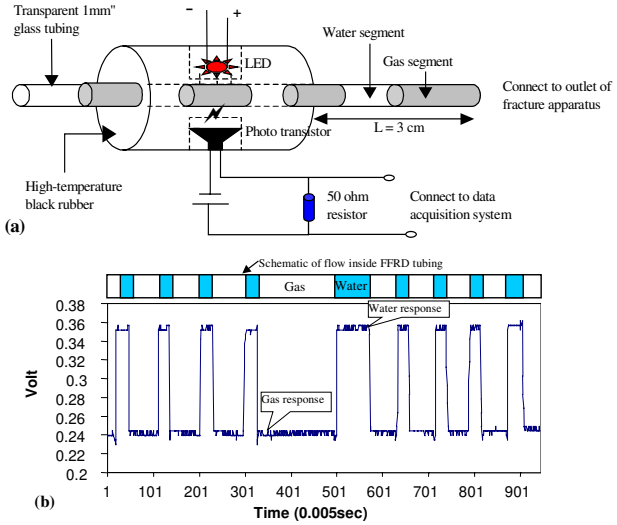

Figure 4. Fractional flow ratio detector (FFRD) (a) schematic (b) detected gas and water signal corresponding to different gas and water segments inside FFRD tubing.

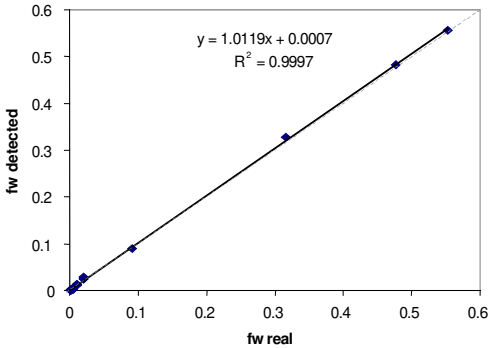

Figure 5. FFRD calibration (Fluids: water and nitrogen gas; FFRD tubing ID: 1.0mm).

3.4 Saturation Measurements

Still images were extracted from digital video recorded during the experiments. The photographs were processed in a Matlab® program. The program does quadratic discriminant analysis (QDA) to divide the pixels of the picture into three groups: water phase, gas phase and the frame. The grouping is

based on color differences. Saturation is calculated as total pixels of the liquid group over the sum of the gas and liquid groups. Figure 6 is a comparison of the gray-scaled image produced by the QDA program and the original photograph from the digital camcorder. Pan et al. (1996) also used a similar technique for measurement of saturation. Their study noted that the source of errors in this technique is the quality of the photographs and the water film adsorbed on the surfaces of the plates with the latter being of minimal effect. Good quality photographs are the ones with clear distinction between the gas and liquid phase. Good lighting is necessary so that the colors in the image come out clearly. The lighting should also be positioned in a way that it does not produce shadow on the flow area. The program will mistakenly take the shadow as gas phase even if there is liquid. From Figure 6, it can be said that the program has good accuracy.

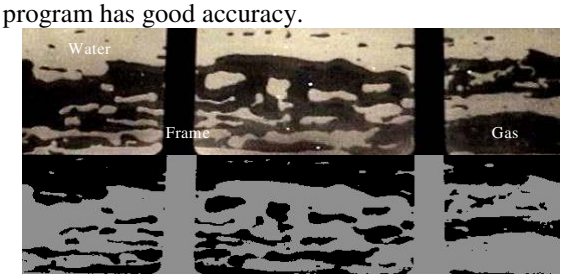

Figure 6. *Comparison between the true color image of the fracture flow and gray scale image from the Matlab QDA program used in measuring saturation.*

3.5 Data Processing

The experiment contains several runs with designated input rates of gas and water. According to the air-water experiments by earlier studies, these fracture flow experiments are not expected to reach a perfect steady state. Instead, they are unsteady by nature. There are significant pressure fluctuations accompanied by saturation changes when the gas and liquid flow rates vary. Due to this behavior, instantaneous outlet rates of gas were also measured by the FFRD device for the relative permeability calculation and flow rate comparison. Digital video was taken in each run when the flow reached steady state or repeated similar fluctuating behaviors. The continuous images of each run were extracted from the video every 0.3 seconds. These hundreds of images in each run were then input into the computer programs for the saturation calculation, flow structure recognition and characterization of the stability of the two-phase flow. The data acquisition task requires frequent gathering of instantaneous and synchronized pressure, flow rate and saturation values. Instantaneous gathering of data was accomplished by the use of the high–speed data acquisition system and digital video camcorder. Video shots were taken of the pressure, time and saturation data displayed all at the same time. Pressure data and related time were displayed by the LCD monitor connected to the computer, which also ran the data acquisition system. The methodology used to integrate all the data and signals and then calculate the gas-water relative permeability is illustrated in the flow chart in Figure 7.

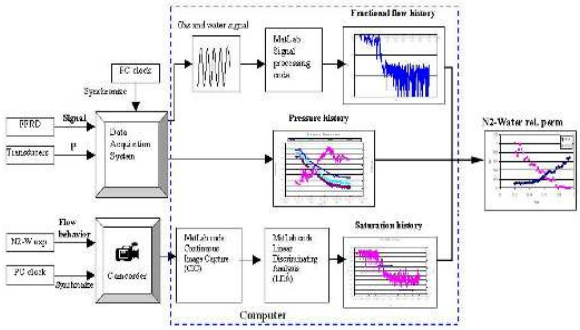

Figure 7. Data and signal processing flowchart.

4 EXPERIMENTAL RESULTS

We first describe the flow structures observed during the experiment, and then present the relative permeabilities calculated at one-second frequency in each run and their averaged values. Finally, we interpret the relative permeabilities using models from earlier studies.

4.1 Description of Flow Structures

The use of a transparent glass plate allows us to observe and videotape the two-phase flow structures. The recorded digital video was then transformed to continuous snapshots with the frequency of 3 images/sec (0.33 seconds period). More than 3000 still images were extracted from the digital video and used for the flow structure characterization and saturation calculation. Several flow structures depending on the flow rates were observed. Generally, when the water saturation decreases, one observes successively bubbles, slugs and channels (Figure 8).

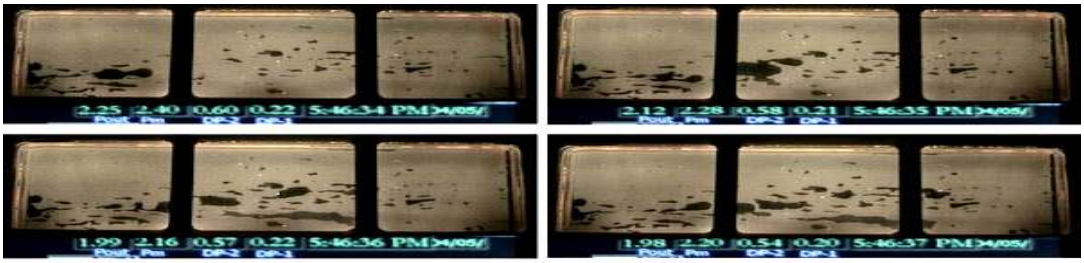

(a) Bubble Flow

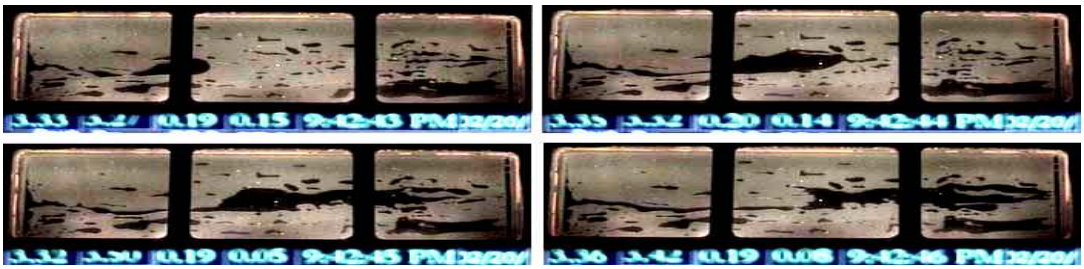

(b) Slug Flow

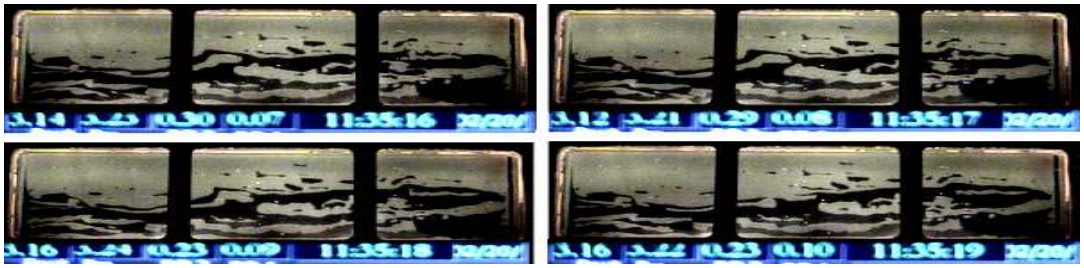

(c) Tortuous Channel Flow

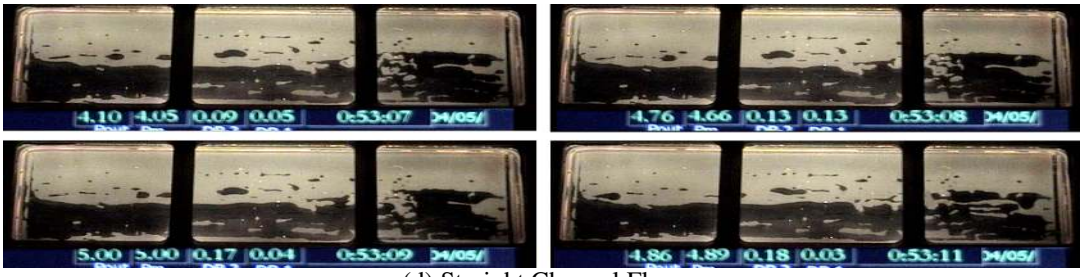

(d) Straight Channel Flow

Figure 8. Photographs of flow structures in the smooth-walled fracture. Each set contains four continuous images. Flow direction was from left to right.

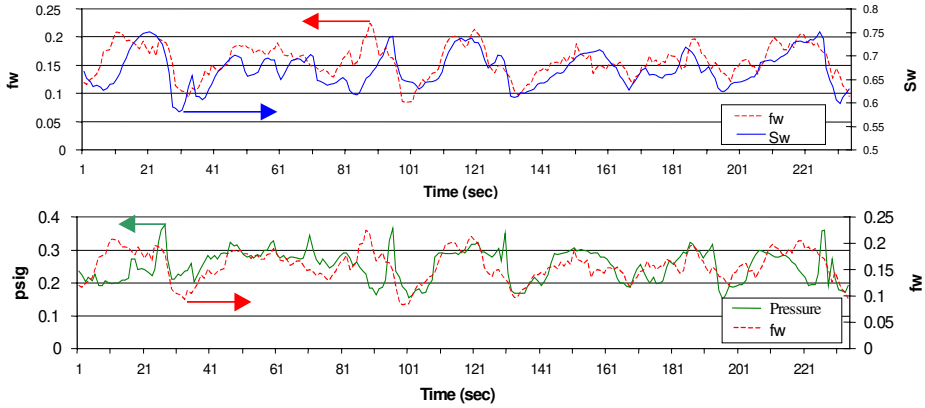

Figure 9. Relationship among water saturation (S_w), water fractional flow (f_w) and pressure difference along the fracture in a highly tortuous channel flow.

The bubble flow is observed only at extremely high values of the water saturation, S_w. Due to the small fracture aperture (130 μm), large gas bubbles propagate either in bullet-like or ellipse-like forms with greater longitudinal length (Figure 8a). As the gas flow rate increases or water flow rate decreases, gas moves in narrow slugs and flows discontinuously when the gas rate is still relatively low as shown in Figure 8b. The higher pressure difference occurs mostly when a slug tries to break through the water region. Once the slug reaches the outlet of the fracture, the pressure difference decreases. This type of slug movement is seen frequently for high values of S_w. With the appearance of bubbles and slugs, the two-phase flow is fairly unstable. When the longitudinal size of slugs increases as the gas rate increases, the moving slugs tend to form stable gas channels and reach a steady condition. However, the steadiness collapses either because water breaks the thinnest throat of the short-lived channel or because of the insufficient gas supply. This causes continuous fluctuations in the saturation, fractional flow and pressure difference.

As the gas rate increases further, the short-lived channel becomes more and more stable. The gas channel meanders through the fracture with branches and junctions because the viscous force is insufficient to break through intermediate water islands. We define this kind of channel as a tortuous channel as shown in Figure 8c. The lifetime of these channels seems to depend on the complexity and meander of their structure. Some tortuous channels might exist just for a few seconds, whereas others exist for long periods. The S_w, f_w and pressure difference histories plotted in Figure 9 are obtained from a tortuous-channel-dominated run. Clearly, even though constant gas and water rates are injected into the fracture, the S_w keeps fluctuating in the fracture and the instantaneous f_w sensed from the FFRD follows this saturation fluctuation as shown in the top plot of Figure 9. The corresponding pressure response was also recorded as shown in the bottom plot of Figure 9. Most of the peaks in these two plots are due to the collapse, reconstruction and reconfiguration of channels, and some intrusions from other minor flow structures (bubbles and slugs). It is also observed that the more tortuous the channel, the larger the pressure difference along the fracture for the same water saturation.

On the other hand, straighter channels were observed more frequently in high f_g situations shown in Figure 8d. In this situation, almost all of the gas flows solely in a fairly straight channel, while most of the water flows above and below the gas path. Except for a small amount of immobile water inside the central gas channel, the gas path is more uniform and less tortuous in comparison with the tortuous channel flow. Three major factors may affect the morphology of gas channels. These factors are the f_g (viscous force), gas-water viscosity ratio (viscous force) and the interfacial tension (capillary force). Therefore for the same S_w, flows with the viscosity ratio closer to one or the smaller interfacial tension have straighter channels.

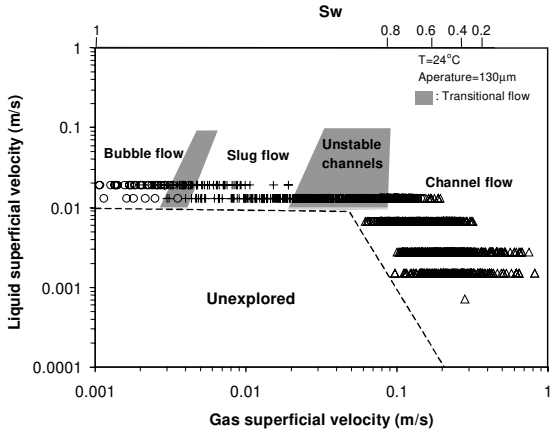

Figure 10. Flow structure map for air-water flow in the smooth-walled fracture.

Figure 10 shows a flow structure map for the experiment. The corresponding S_w is also provided in this figure. It is easy to see that the channel flow spans most of the S_w range and major bubble and slug flows only exist in high S_w situations. The shadow areas in the flow maps indicate transitional flow which means the flow structure is a combination of the two neighboring structures. The transition between the slug flow and channel flow is defined as unstable channel flow. In this region, some large fingering slugs were able to bridge the two ends of the fracture. However, the bridged slug collapsed in a short time due to its unstable structure, water intrusion and the insufficient gas supply. The flow structure map is similar to the flow map (glass fracture) presented by Fourar and Bories (1995).

4.2 Relative Permeability Calculations

The absolute permeability of the smooth-walled fracture was first measured in single-phase water flow. The absolute permeability of the fracture deduced from measurements by using the Darcy equation is 1.51×10^{-9} m^2 (1510 darcies). The gap width (aperture) of the fracture is 130 μm, the estimated permeability from Equation (4) is then 1.41×10^{-9} m^2 (1410 darcies). As can be seen in Figure 11, measured values are in a good agreement with the theoretical value of the absolute permeability.

Air-water relative permeabilities were calculated by using Equations (1) and (3) at one-second frequency in each run. The instantaneous flow rate was obtained from the FFRD. Comprehensive air-water relative permeabilities obtained from thousands of data points are plotted in Figure 12. Data points in the figure show acceptable correlation. Comprehensive water

relative permeabilities are scattered at high water saturation owing to the slug and unstable-channel flows in the gas-phase as shown in Figures 8a and 8b. The vertically scattered effect observed with the gas-phase relative permeability under extremely low values of water saturation may be associated with either the pressure fluctuation due to the moving water slugs or the difficulty in sensing the instantaneous f_w from the FFRD at low f_w.

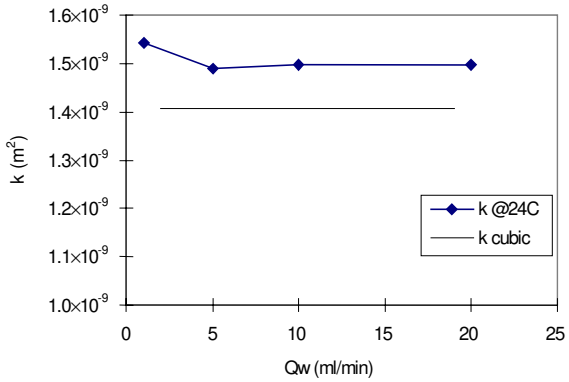

Figure 11. Absolute permeability of the fracture (aperture = 130 μm).

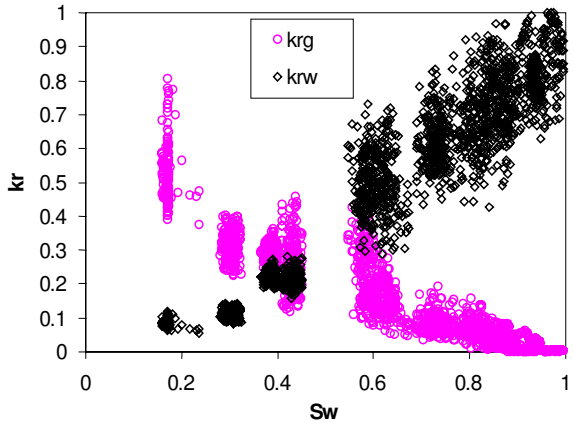

Figure 12. Comprehensive air-water relative permeabilities in the smooth-walled fracture.

4.3 Relative Permeabilities Interpretation

The averaged values of the relative permeabilities and the saturation for each pair of liquid and flow rates are presented in Figure 13. Also plotted in this figure are the curves of the X-model (Equations (5) and (6)), the Corey-model (Equations (7) and (8)) with S_{rl} = 0 and S_{rg} = 0, and the viscous-coupling model (Equations (10) and (11)). It appears that the X-model does not fit the experimental data. For a given value of S_w, the k_{rl} and k_{rg} are below the straight lines. Although gas-phase experimental values are closer to the Corey curve, water-phase values are much higher than the water-phase Corey curve. Therefore, neither the Corey curve nor the X-curve can fit the experimental result. On the other hand, the viscous-coupling model is in a good agreement with experimental results, especially for the water-phase. For the gas phase, the viscous-coupling model shows acceptable fitting, but it seems to be less accurate at high water saturation. The photographs in Figure 8 provide some clue about this less accurate result. At high values of S_w, most of the water channels extend from longitudinal boundaries of the fracture space and flow straighter and more continuously. On the other hand, the active gas flows as fingering slugs and channels with amorphous shapes. These changing shapes generate the corresponding pressure, saturation and flow rate changes as illustrated in Figure 9. The relative permeability may be affected by these changes that are not considered by the previous models (X, Corey and viscous-coupling). The further study of flow structure effects on relative permeabilities will be presented in the next section.

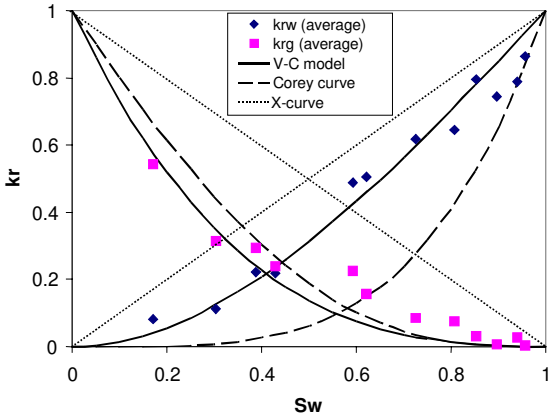

Figure 13. Comparison of average experimental relative permeability with the Corey-curve, X-curve and viscous-coupling models.

5 EFFECTS OF FLOW STRUCTURES ON RELATIVE PERMEABILITIES

Figure 10 shows that the channel flow is the dominant flow structure in our experiments. We might expect that these flows would be described by the X-model. Instead, they are rather in accordance with the viscous-coupling model. This can be explained by characterizing the morphology of phase channels and quantifying the magnitude of the "tortuosity" in this flow structure. A new approach will be discussed here to include the tortuosity created by the phases.

5.1 Tortuous-Channel Approach

Considering a simplified fracture space with a dimension of L (length) × W (width) × b (aperture) as shown in Figure 14, the fluids, water and gas, form ideal and straight channels through the fracture. From fundamentals of multiphase flow, the X-curve behavior is readily derived from Darcy's law and the cubic law by assuming negligible capillary pressure,

gas slippage, inertia effect and wetting-phase stratified flow.

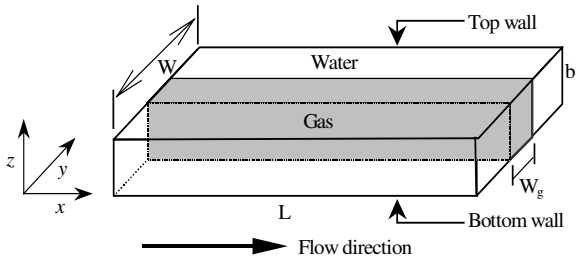

Figure 14. A simple model of a straight gas channel in a smooth-walled fracture.

Consequently, the straight phase-channel in the smooth-walled fracture will yield the X-curve relative permeability as shown by Romm (1966). However, as shown in this study, the actual flow structures in fractures seldom reach the ideal straight channel even though the fracture is smooth-walled. Most of the flow structures are either fingering or tortuous channels instead, and the relative permeability obtained from this experiment shows a deviation from X-curve as presented earlier in Figure 13. As a result, a physical, tortuous-channel approach to modify X-curve and take into account the channel tortuosity is required.

The concept of the tortuous-channel approach is based on the relationship between the fluid tortuosity and the relative permeability. As the channel flow observed in our study is tortuous (Fig. 9c), we define a tortuosity coefficient for the channel flow, τ_c, to characterizing its morphology. The definition of this apparent parameter is based on the area of the channel and the smallest bounding rectangle that covers the whole channel for a specific phase. As shown in Figure 15, the binary images processed from continuous true-color images were input into another image-processing program, which allows recognition and separation of the different flow structures. Then, the channel area, A_c (unit: pixel^2), length and width of the smallest bounding box, L_x and L_y (unit: pixel), were computed. The channel tortuosities for gas and water are then defined as:

$$\tau_{c,g} = \left(\frac{L_x L_y}{A_c}\right)_g \text{ and } \tau_{c,w} = \left(\frac{L_x L_y}{A_c}\right)_w \qquad (14)$$

As for the relative permeability, coefficient τ_c for each phase varies between 1 and ∞. This coefficient is related to the interfacial area and, consequently, allows quantifying the shear stress at the interface between the two fluids.

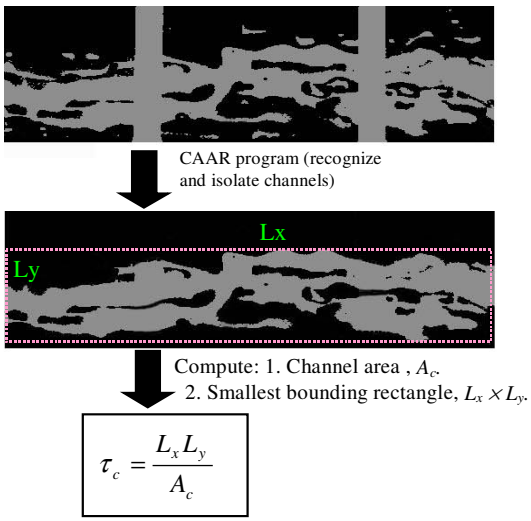

Figure 15. Evolution of channel tortuosity algorithm.

In this study, thousands of continuous images extracted from the video of the experiment with a 0.33 second period were analyzed, and the tortuosities of gas and water were deduced for the channel flow configuration. Illustrations of these calculations are presented in Figure 16. It appears that water channels are less tortuous than gas channels. This may be due to the fact that the water-viscosity is higher than the gas-viscosity, and that water channels tend to adhere to longitudinal boundaries of the fracture, while gas channels flows in between.

In order to characterize the deviation from the X-model, we propose the following relationships:

$$k_{rw} = \frac{S_w}{\tau_{c,w}} \qquad (15)$$

$$k_{rg} = \frac{S_g}{\tau_{c,g}} \qquad (16)$$

This relationship assumes that the channel tortuosity is directly proportional to the deviation of X-curve behavior. In the case where each phase flows in the form of homogeneous strata (no dispersed phase), τ_{cw} = 1 and τ_{cg} = 1 and Equations (15) and (16) reduce to the X-model.

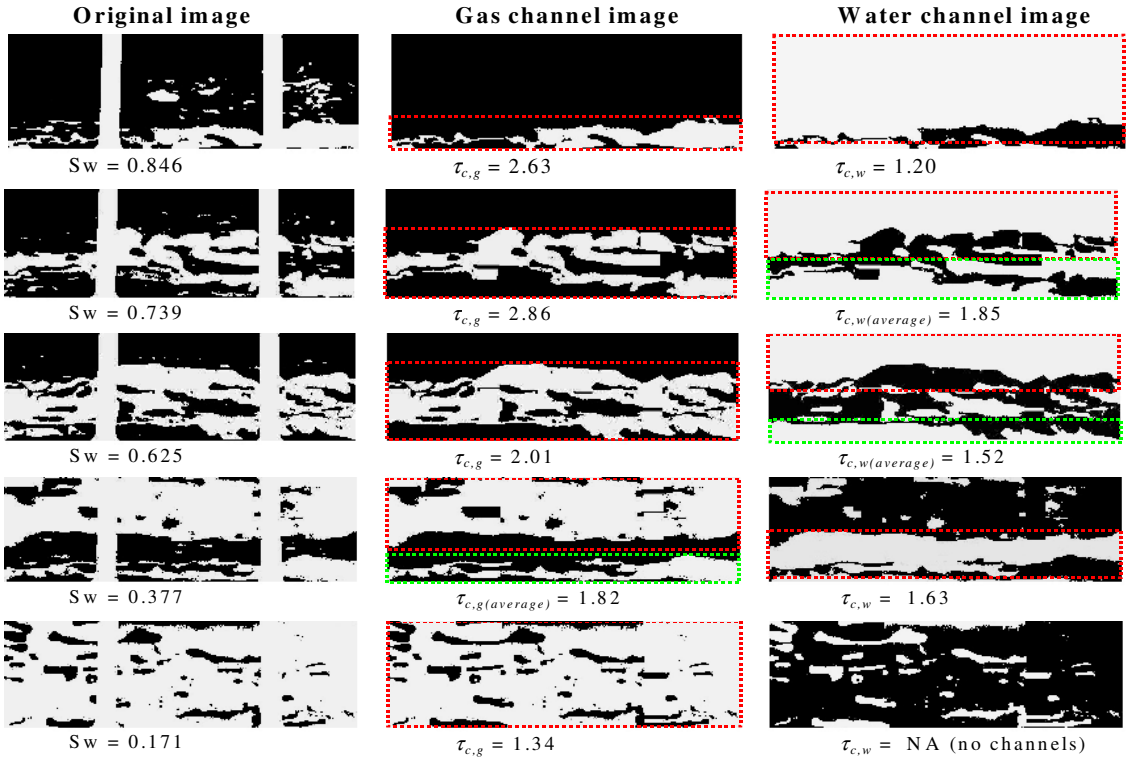

Figure 16. Representative images and corresponding processed gas-channel and water-channel images extracted from the CAAR image processing. (Phase channels are in white color in the channel images. Rectangles indicate the bounding boxes of the phase channels.)

5.2 Reproduction of Relative Permeabilities

After deducing both water and gas tortuosities from the extracted images, the comprehensive water-phase and gas-phase relative permeabilities obtained from Equations (15) and (16) are shown in Figure 17. The original experimental results (Figure 12) are also provided in this figure. The results from the tortuous-channel approach show good reproduction of the experimental results in both water and gas phases. Thus, the tortuous-channel approach leads to low scatter in comparison with the experimental relative permeabilities. This is because some unstable phenomena, bubbles and slugs, were excluded and there are almost no sources of measurement errors in the tortuous-channel approach, except the image processing errors.

The mean tortuosity of gas and water channels was then computed by averaging all tortuosities in each run. Table 1 presents the mean channel tortuosity in each run for the experiments. The average phase tortuosity (reciprocal) versus the phase saturation is shown in Figure 18. Values of tortuosity reciprocal approach 1.0 when the channels increase straightness. A tortuosity value (or reciprocal) of 1.0 means perfect straight phase channels. From these two plots, it is evident that the higher the phase saturation, the less tortuously those phase channels behave. The phase tortuosity values can be expressed by their phase saturations in second order approximations. The relative permeabilities calculated by using the average tortuosity in Table 1 and Equations (15) and (16) are presented in Figure 19. They are in a good agreement with average experimental relative permeabilities for both gas and water phases. Aside from the generally matching performance, the tortuous-channel approach not only approximates the experimental result but closely reproduce some experimental points, especially the portion where the viscous-coupling model performs poorly.

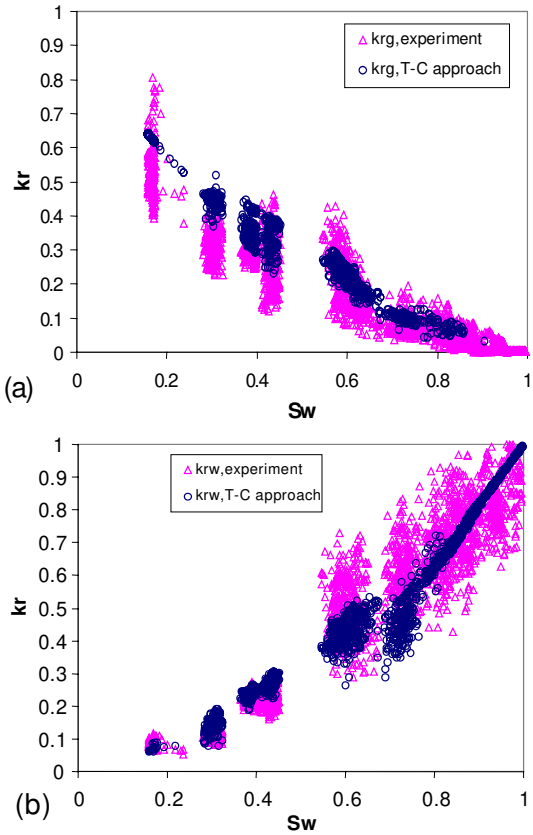

Figure 17. Relative permeabilities from tortuous-channel approach using phase tortuosities obtained from the processing of continuous images and its comparison with the original result: (a) gas phase, (b) water phase.

Table 1. Averages of tortuous-channel parameter obtained from CAAR image processing program and the relative permeavility values for the tortuous-channel approach and experiment.

Saturation		Average channel tortuosities		Experiment results		Tortuous-channel approach	
S_w	S_g	$\tau_{c,g}$	$\tau_{c,w}$	$krg,_{expe}$	$krw,_{expe}$	$krg,_{T\text{-}C}$	$krw,_{T\text{-}C}$
0.957	0.043	NA*	1.038	0.002	0.863	NA	0.922
0.941	0.059	NA	1.065	0.028	0.788	NA	0.884
0.897	0.103	2.476	1.098	0.007	0.743	0.041	0.817
0.854	0.146	2.6	1.143	0.03	0.794	0.056	0.747
0.807	0.193	2.771	1.246	0.077	0.646	0.069	0.648
0.726	0.274	2.797	1.61	0.086	0.619	0.098	0.451
0.622	0.378	2.033	1.434	0.158	0.506	0.186	0.434
0.592	0.408	1.699	1.437	0.225	0.487	0.24	0.412
0.43	0.57	1.702	1.54	0.239	0.217	0.335	0.279
0.387	0.613	1.746	1.639	0.294	0.221	0.351	0.236
0.304	0.696	1.583	2.051	0.315	0.112	0.44	0.148
0.171	0.829	1.337	2.464	0.541	0.083	0.62	0.069

*: No channel detected.

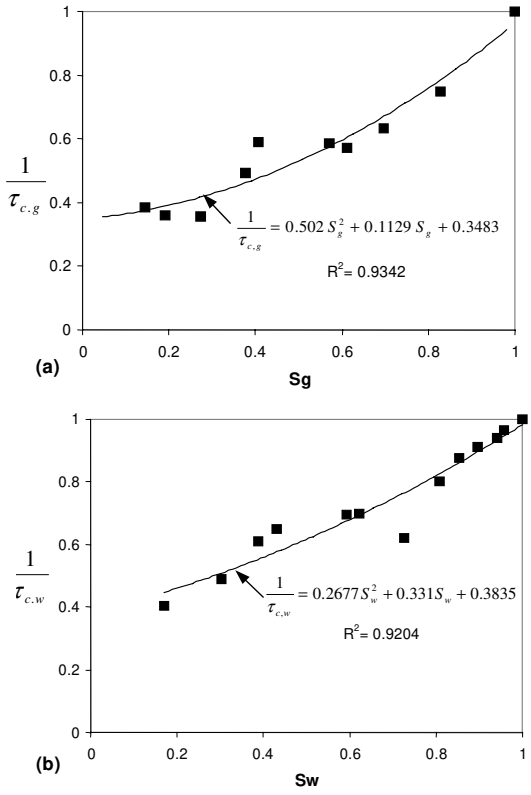

Figure 18. Reciprocal of average phase-channel tortuosity versus phase saturation in the air-water experiment: (a) gas phase, (b) water phase

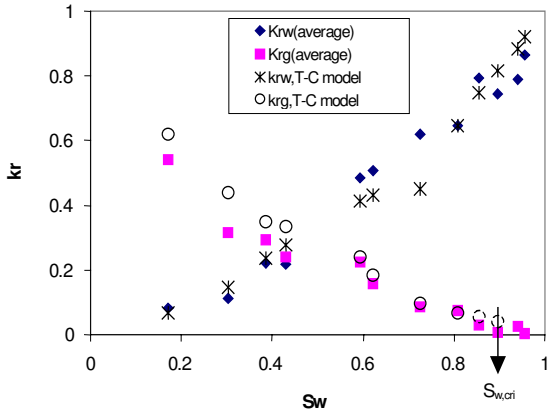

Figure 19. Comparison of average relative permeabilities from the tortuous-channel approach and from experiment. (The dash circles may contain more uncertainty due to few sampling points.)

5.3 Comparison with Models

To compare the proposed tortuous-channel approach with other theoretical and empirical models mentioned previously, simple curve fits to express the tortuosity of phase channels mathematically were done in this preliminary stage. The optimal equations for fitting phase tortuosities as shown in Figure 18 are:

$$\frac{1}{\tau_{c,w}} = 0.2677S_w^2 + 0.331S_w + 0.3835 \quad (17)$$

$$\frac{1}{\tau_{c,g}} = 0.502S_g^2 + 0.1129S_g + 0.3483 \quad (18)$$

This leads Equations (15) and (16) to a tortuous-channel model:

$$k_{rw} = 0.2677S_w^3 + 0.331S_w^2 + 0.3835S_w \quad (19)$$

$$k_{rg} = 0.502S_g^3 + 0.1129S_g^2 + 0.3483S_g \quad (20)$$

Figure 20 shows the comparison of the tortuous-channel model and viscous-coupling model. These two models perform equally accurate for the water phase. For the gas phase, the tortuous-channel model fits the experimental data better in high S_w range. On the other hand, the viscous-coupling model shows better performance in low S_w range. This model transition may indicate that the dominant force shifts from the horizontal (*xz*-plane) shear stress to vertical (*xy*-plane) shear stress. The referred coordinate system is illustrated in Figure 14. Considering the gas phase, except in low S_w range, most of the force contributed by the flow was applied for exploring and sustaining the gas region horizontally. Therefore, the magnitude of the vertical shear stress was relatively small and negligible. This leads to the feasibility of using the tortuous-channel approach. However, when most of the fracture space was occupied by the gas at low S_w, less force was used to sustain the gas region horizontally since the gas channels were extended and straighter. Instead, most of the force was contributed by the vertical shear force because of the importance of the vertical stratified flow at this stage. This will be close to the viscous-coupling behavior.

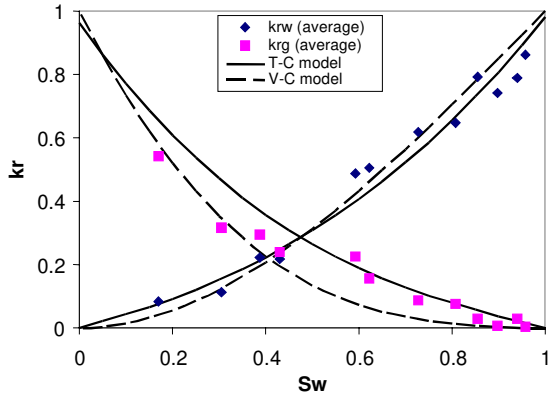

Figure 20. Comparison of the experimental relative permeability with the tortuous-channel model and viscous-coupling model for the air-water experiment.

To compare these models visually and quantitatively, the comparison between measured and predicative water saturation and relative permeabilities was made using Equations (5) to (11) and Equations (19) and (20). The result is shown in Figure 21. The statistical analysis of the absolute errors and standard deviations between experimental and modeling relative permeabilities and saturations is also presented in Table 2. Apparently, both the viscous-coupling model and tortuous-channel model can interpret and predict the relative permeability and water saturation with good accuracy, whereas both the X-curve and Corey-curve models show worse performance. From the statistical mean absolute error and standard deviation, the tortuous-channel model performs slightly better than the viscous-coupling model in predicting both relative permeability and water saturation. To sum up, from validations of both the comprehensive and average results and model comparisons, the proposed tortuous-channel approach can interpret the relative permeabilities at the air-water experiment successfully. This tells us that the relative permeability is flow structure dependent. At the moment, the flow structure prediction is a complicated and immature subject.

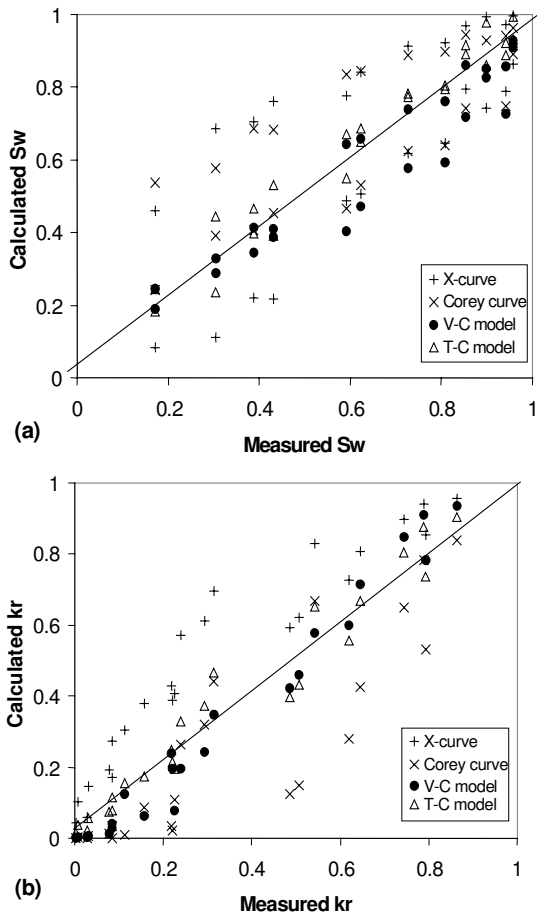

Figure 21. Comparison between measured and calculated (a) water saturation, (b) relative permeavility.

Table 2. Statistical analysis descriptors (mean absolute error and standard deviation) of relative permeabilities and water staturation between experiment and models.

Models	k_r		S_w	
	$MAE^{\dagger}(k_r)$	$\sigma^{\ddagger}$	$MAE(S_w)$	σ
X-curve	0.1633	0.0920	0.1633	0.0920
Corey curve (Corey, 1954)	0.1207	0.1147	0.1313	0.1008
Viscous-coupling model*	0.0496	0.0377	0.0729	0.0653
Tortuous-channel model (this work)	0.0485	0.0384	0.0505	0.0325

* : Fourar and Lenormand, (1998)

† : Mean absolute error; $MAE(Y) = \frac{1}{N}\sum_1^N \left|Y_{\exp e,i} - Y_{\mathrm{mod}\,el,i}\right|$

‡ : standard deviation, $\sigma = \sqrt{\frac{1}{N-1}\sum_1^N \left(\left|Y_{\exp e,i} - Y_{\mathrm{mod}\,el,i}\right| - MAE(Y)\right)^2}$

6 CONCLUSION

Experimental results of air-water flow through a smooth-walled fracture were presented. Using a high-speed data acquisition system and digital image processing technology, the experimental apparatus was able to characterize the unstable nature of the flow.

Different flow configurations were visualized: bubbles, slugs and channels. Experimental results of pressure drop, flow rates, and saturation were interpreted by using the relative permeability concept and compared to three models from the literature: the X-model, the Corey-model and the viscous-coupling model. The results were well described by the viscous-coupling model showing more interactions between phases than the X-model, but less interference than predicted by the Corey-model.

By introducing the tortuous-channel concept, we showed that the deviation from the X-model is due to the flow configuration. The proposed tortuous-channel approach has reproduced both original and average experimental relative permeabilities. After applying mathematical expressions of phase tortuosity coefficients, the preliminary tortuous-channel model performed best among other models. Therefore the concept of the tortuosity coefficient may allow modeling two-phase flow in a fracture whatever the flow configuration. To this end, the coefficient τ_c must be related physically to the shear stress at the surface between the two fluids and to the interface area. Unfortunately, up to now there is no model that allows us to predict flow structures in a fracture. It was also noticed that the values of the gas-phase relative permeability from the experiment tend to shift from the proposed tortuous-channel model to the viscous-coupling model in the low water saturation range, which may be because the vertical stratified flow is no longer negligible in this situation.

Acknowledgement

Financial support for this research was provided by the US Department of Energy under contract DE-FG07-02ID14418. The authors would like to thank Dr. Kewen Li for helpful discussions.

REFERENCES

Brooks, R. H. and Corey, A. T., Properties of Porous Media Affecting Fluid Flow, *J. Irrig. Drain. Div*., 6, 61, 1996.

Chen, C.-Y., Diomampo, G., Li, K. and Horne, R.N., Steam-Water Relative Permeability in Fractures, *Geothermal Resources Council Transactions Vol.26*, pp. 87-94, 2002.

Corey, A. T., The Interrelation between Gas and Oil Relative Permeabilities, *Prod. Mon*., **19**, 38, 1954.
Diomampo, G., *Relative Permeability through Fractures*, MS thesis, Stanford University, Stanford, California, 2001.

Fourar, M. and Bories, S., Experimental Study of Air-Water Two-Phase Flow Through A Fracture (Narrow Channel), *Int. J. Multiphase Flow* Vol. 21, No. 4, pp. 621-637, 1995.

Fourar, M., and Lenormand, R., A Viscous Coupling Model for Relative Permeabilities in Fractures, Paper SPE 49006, Presented at the SPE Annual Technical Conference and Exhibition, New Orleans, Louisiana, USA, September 27-30, 1998.

Mendoza, C.A. and Sudicky, E.A., Hierarchical scaling of constitutive relationships controlloing multi-phase flow in fractured geologic media, paper presented at the Third Int. Conf. on Reservoir Characterization Requirements for Different Stages of Development, Tulsa, OK, 1991.

Murphy, J.R. and Thomson, N.R., Two-Phase Flow in a Variable Aperture, *Water Resources Research*, vol. 29, No 10, pp. 3453-3476, 1993.

Persoff, P. K., Pruess, K., and Myer, L., Two-Phase Flow Visualization and Relative Permeability Measurement in Transparent Replicas of Rough-Walled Rock Fractures, *Proc. 16th Workshop on Geothermal Reservoir Engineering*, Stanford University, Stanford, California, January 23-25, 1991.

Persoff, P., and Pruess, K., Two-Phase Flow Visualization and Relative Permeability Measurement in Natural Rough-Walled Rock Fractures, *Water Resources Research* Vol. 31, No. 5, May, pp. 1175-1186, 1995.

Pan, X., Wong, R.C., and Maini, B.B., Steady State Two-Phase Flow in a Smooth Parallel Fracture, presented at the 47th Annual Technical Meeting of the Petroleum Society in Calgary, Alberta, Canada, June 10-12, 1996.

Pyrak-Nolte, L.J., Helgeston, D., Haley, G.M., and Morris, J.W., Immiscible fluide flow in fracture, *Proceeding of the 33rd U.S. Rock Mech. Symp.,* edited by Tillersson and Wawersik, pp. 571-578, A. A. Balkema, Rotterdam, Netherlands, 1992.

Romm, E.S., *Fluid Flow in Fractured Rocks,* "Nedra" Publishing House, Moscow, 1966 (Translated from the Russian).

Rossen, W.R., and Kumar A.T.A., Single and Two-phase flow in natural fractures, SPE 24195, the 67th SPE Annual Technical Conference and Exhibition, Washington D.C., Oct. 4-7, 1992.

Scheidegger, A.E., *The Physics of Flow Through Porous Media*, 3rd ed., University of Toronto, Toronto. 1974.

Witherspoon, P.A., Wang, J.S.W., Iwai, K. and Gale, J.E., Validity of Cubic Law for Fluid Flow in a Deformable Rock Fracture, *Water Resources Research*, Vol. 16, No. 6, pp 1016-1024, 1980.

Yih, C.S., *Fluid Mechanics*, McGraw-Hill, New York. 1969.